Journal of ELECTRONIC MATERIALS, Vol. 48, No. 10, 2019
https://doi.org/10.1007/s11664-019-07445-7

Junction Parameters and Electrical Characterization of the Al/n-Si/Cu_2CoSnS_4/Au Heterojunction

I.M. EL RADAF,[1,2,6] H.I. ELSAEEDY,[3] H.A. YAKOUT,[3,4] and MARDIA T. EL SAYED[5]

1.—Physics Division, Electron Microscope and Thin Films Department, National Research Centre, Dokki, Giza 12622, Egypt. 2.—Materials Physics and Energy Laboratory, College of Sciences and Art at ArRass - Qassim University, ArRass 51921, Kingdom of Saudi Arabia. 3.—Department of Physics, Faculty of Science, King Khalid University, Abha, Kingdom of Saudi Arabia. 4.—Department of Material Science, Institute of Graduate Studies and Research, Alexandria University, Bab Sharqi, Egypt. 5.—Chemical Industries Research Division, Applied Organic Chemistry Department, National Research Centre, 33 EL Buhouth St., Dokki, Giza 12622, Egypt. 6.—e-mail: elradaf11b@gmail.com

Quaternary kesterite thin films of Cu_2CoSnS_4 were deposited on the n-Si substrate to fabricate Cu_2CoSnS_4/n-Si heterojunctions. The x-ray diffraction and field emission scanning electron microscopy were employed to study the structural properties of the Cu_2CoSnS_4 deposited on to n-Si single crystal substrate. The capacitance–voltage measurements of the Cu_2CoSnS_4/n-Si heterojunction were investigated to study the junction nature which displays an abrupt junction. The dark *I*–*V* characteristics of the Cu_2CoSnS_4/n-Si heterojunction displays a rectification behavior. We characterized the influence of the annealing temperature on the magnitudes of the diode parameters of the Cu_2CoSnS_4/n-Si heterojunction. The barrier height ϕ_b of the Cu_2CoSnS_4/n-Si heterojunction was increased with raising the annealing temperature while the ideality factor n has a reverse performance. The illuminated *J*–*V* plot of the Cu_2CoSnS_4/n-Si heterojunction displays an efficiency of 6.17% for the prepared junction.

Key words: Copper cobalt tin sulfide, spray pyrolysis technique, XRD, FE-SEM, photovoltaic, *I*–*V* and *C*–*V* characteristics, heterojunction

INTRODUCTION

Recently, Earth-abundant kesterite thin films like Cu_2ZnSnS_4, Cu_2CdSnS_4, Cu_2FeSnS_4, Cu_2MnSnS_4, and Cu_2CoSnS_4 attracted high interest in the last years owing to they are inexpensive, nontoxic, more abundant and exhibit good optical and electrical properties.[1–3] These materials exhibit a *p*-type conductivity and excellent optoelectronic properties, so they are ideal absorber materials for solar cells.[4] The high stability of the kesterite thin films makes it suitable for various applications like solar cells and photonic devices.[5] Cu_2ZnSnS_4 films display a high absorption coefficient and a suitable band gap so they are considered a good competitor for CdTe and $CuIn_xGa_{1-x}S_2$ in the fabrication of solar cells. The Cu_2ZnSnS_4 solar cell reached an efficiency of 12%.[6] So, the study of the other kesterite thin films, such as Cu_2CdSnS_4, Cu_2FeSnS_4, Cu_2MnSnS_4, and Cu_2CoSnS_4 is very important to fabricate low-cost solar cells. Cu_2CoSnS_4 is an alternative solar absorber with excellent optical, thermoelectric and magnetic properties which is well suited for utilization in solar energy conversion.[7] Different preparation techniques were utilized to fabricate the Cu_2CoSnS_4 powder and thin films like spray pyrolysis,[8] hydrothermal,[9] solvothermal,[10] sol–gel method,[11] and hot injection[12] techniques. The previous articles are available for studying the structural and optical

(Received March 20, 2019; accepted July 9, 2019; published online July 22, 2019)

properties of the CCTS thin films while there is no interest in the fabrication of CCSS/n-Si heterojunction. So, the present work is aimed to fabricate and study the structural and electrical properties of the Cu_2CoSnS_4/n-Si heterojunction synthesized by spray pyrolysis method. The junction parameters of the Cu_2CoSnS_4/n-Si heterojunction have been estimated from the current–voltage characteristics curve. The junction nature and the donor carrier concentrations of the Cu_2CoSnS_4/n-Si heterojunction were evaluated from the capacitance–voltage characteristics in the dark.

EXPERIMENTAL DETAILS

Synthesis of the Cu_2CoSnS_4 Thin Film and Heterojunction

High quality Cu_2CoSnS_4 thin film was synthesized by the interaction between 0.1 M copper chloride dehydrate, 0.05 M cobalt chloride dehydrate, 0.05 M stannic chloride dehydrate and 0.2 M thiourea. A mixture of propanol to water ratio of 1:3 ml has been used for solution preparation. The pH of the solution set at 10. The final Cu_2CoSnS_4 solution was sprayed into a heated glass substrate held at 300°C. For heterojunction fabrication, an *n*-type Si substrate was chemically etched by a mixture of different acids (HF:HNO_3:CH_3COOH) with a ratio of 1:6:1[13] Then the n-Si substrate was cleaned well with deionized water then dried. After the cleaning process, an Al film with a thickness of 200 nm was deposited on the bottom side of the n-Si substrate. A Cu_2CoSnS_4 thin film of thickness 479 nm was sprayed on the top surface of the n-Si substrate by spray pyrolysis system. Then Au electrode with a thickness of 200 nm was deposited on the surface of the Cu_2CoSnS_4 thin film. The Al and Au electrodes were performed by a thermal evaporation technique type (Edward 306 A). Figure 1 displays the Al/n-Si/Cu_2CoSnS_4/Au heterojunction.

Characterization of the Cu_2CoSnS_4 Thin Film and Heterojunction

XRD scan was carried out to examine the structure of the Cu_2CoSnS_4 thin film. Quanta FEG 250 field emission scanning electron microscopy was used to scan the surface morphology of the Cu_2CoSnS_4 thin film. A computerized *C–V* meter was used to study the dark capacitance–voltage (*C–V*) characteristics of the Al/n-Si/Cu_2CoSnS_4/Au heterojunction. A programmable electrometer (Type Keithley-2635 A) was employed to measure the current–voltage *I–V* characteristics of the Al/n-Si/Cu_2CoSnS_4/Au heterojunction. A halogen lamp was employed for the illumination process. A solar power meter was used to measure the intensity of the incident light.

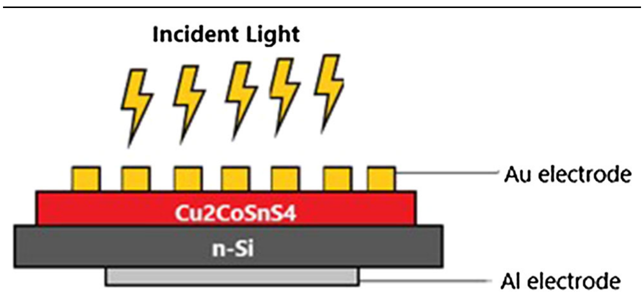

Fig. 1. Schematic diagram of Al/n-Si/Cu_2CoSnS_4/Au heterojunction.

RESULTS AND DISCUSSION

Structural Characterizations

Morphology and EDAX of the Cu_2CoSnS_4 Thin Film

Representative surface morphology image of the Cu_2CoSnS_4 film is presented in Fig. 2. The morphology of the Cu_2CoSnS_4 layer displayed that the film has a crack-free smooth surface and formed from spherical grains. The EDAX pattern demonstrated that the existence of Cu, Co, Sn and S in the Cu_2CoSnS_4 film and its atomic ratio are Cu = 21.62, Co = 11.43, Sn = 10.16, S = 38.84 and Si = 17.95 at.%, respectively.

XRD Study

The XRD pattern of the Cu_2CoSnS_4 thin film grown on the n-Si substrate is presented in Fig. 3. The pattern shows that Cu_2CoSnS_4 thin films are polycrystalline in nature. The previous work illustrates that the Cu_2CoSnS_4 thin films exhibit tetragonal structure. Maldar et al.[14] demonstrated that Cu_2CoSnS_4 thin films prepared by spray pyrolysis reveal a tetragonal phase. Mokurala et al.[15] confirmed that Cu_2CoSnS_4 thin films fabricated by spin coating display a tetragonal phase. In this work, the study of the diffraction pattern of the Cu_2CoSnS_4 thin films displays that the appeared planes were matched with the tetragonal crystal structure Cu2CoSnS4 phase according to JCPDS card No. 26-0513.

The structural constants of the Cu_2CoSnS_4 film represented in the crystallite size (D), the lattice strain (ε), and dislocation density (δ) have been given via the following Scherer's formulas[16–18]:

$$D = \frac{0.9\lambda}{\beta\cos(\theta)}, \quad (1)$$

$$\varepsilon = \frac{\beta\cos(\theta)}{4}, \quad (2)$$

$$\delta = \frac{1}{D^2}. \quad (3)$$

Here β denotes and the experimental full width at the half maximum (FWHM) in radians and θ represents the Bragg diffraction angle.

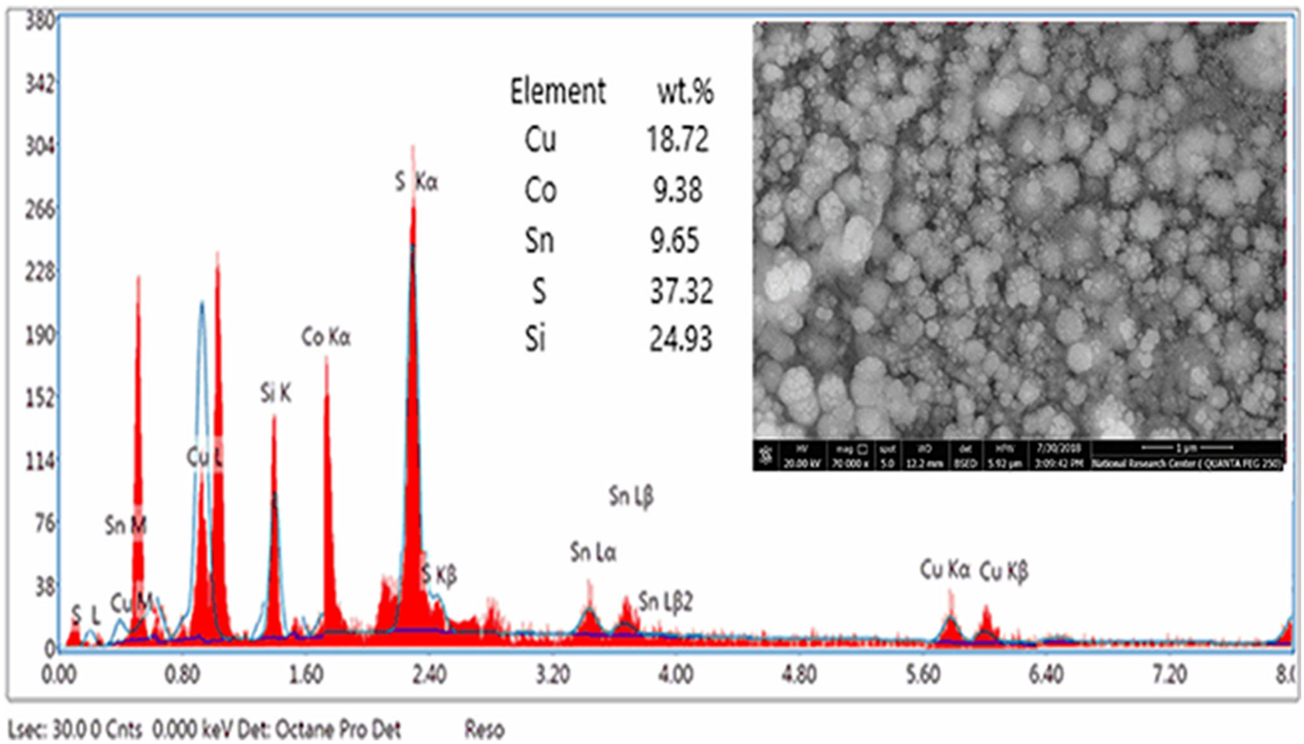

Fig. 2. The FE-SEM and EDAX spectrum of the Cu_2CoSnS_4 thin film deposited on the n-Si substrate.

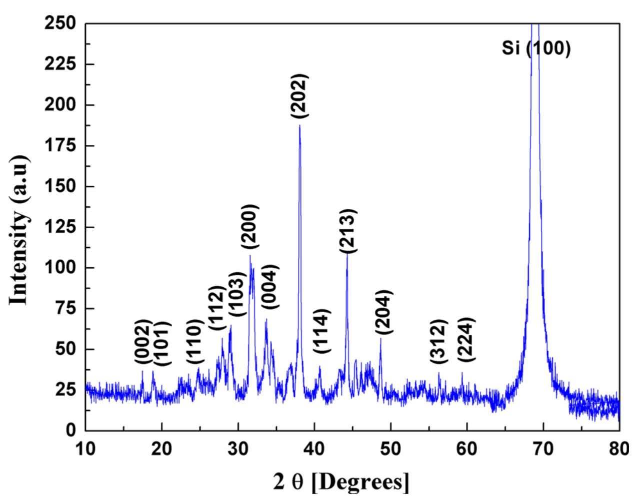

Fig. 3. XRD of the sprayed Cu_2CoSnS_4 thin film fabricated on the n-Si substrate.

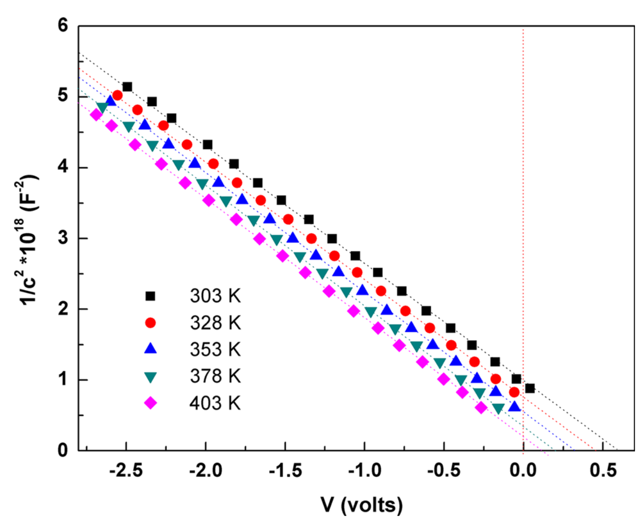

Fig. 4. The dark *C–V* characteristics of the Al/n-Si/Cu_2CoSnS_4/Au heterojunction.

The magnitudes of the structural constants D, ε and δ of the Cu_2CoSnS_4 thin film are 47.68 nm, 3.047×10^{-3} and 4.39×10^{-4} nm^{-2} respectively.

Capacitance–Voltage Characterizations

The Capacitance–Voltage (C–V) measurements of the Cu_2CoSnS_4/n-Si heterojunction occurred at 1 MHz in the dark condition. The C^{-2}–V curve of the Cu_2CoSnS_4/n-Si heterojunction is presented in Fig. 4. The curve displays a linear relation, which revealed that the junction exhibits an abrupt nature. The dependence of the junction capacitance on the reverse bias potential for the Cu_2CoSnS_4/n-Si heterojunction was given via[19,20]:

$$C^2 = \frac{qN_A N_D \varepsilon_1 \varepsilon_2}{2(\varepsilon_1 N_A + \varepsilon_2 N_D)} \frac{1}{(V_{bi} - V)}. \quad (4)$$

Here ε_1 denotes the dielectric constant of the Si substrate and equal 1.044×10^{-11} F cm^{-1}, q

Table I. The magnitudes of the V_{bi} and N evaluated from the dark *C–V* characteristics for the (Al/n-Si/Cu_2CoSnS_4/Au) heterojunction

T (K)	V_{bi} (V)	N *10^{19} (cm^{-3})
308	0.54	3.91
323	0.432	4.28
343	0.35	5.31
353	0.217	5.87
373	0.13	6.26

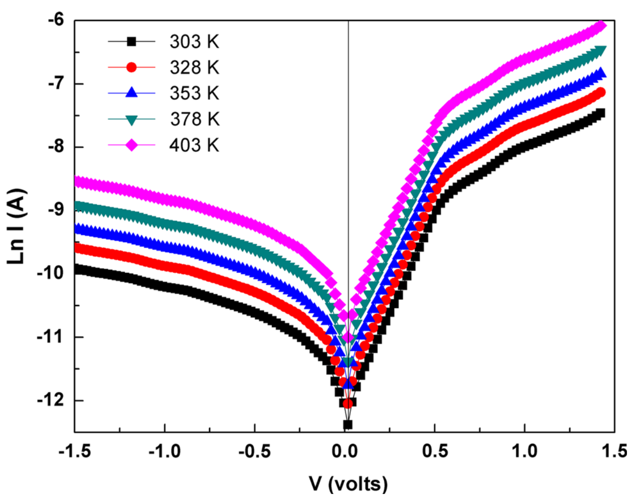

Fig. 5. Forward and reverse *I–V* characteristics of the Al/n-Si/Cu_2CoSnS_4/Au heterojunction in the dark conditions.

denotes the charge of the electron and equals 1.6×10^{-19} C, N_D denotes the donor concentration of n-Si and equal 10^{15} cm^{-3}, N_A denotes the acceptor concentration of the Cu_2CoSnS_4 and ε_2 denotes the dielectric constant of the Cu_2CoSnS_4 thin film.

By extrapolating the line in the Fig. 4 to C^{-2} =0, the built-in voltages V_{bi} of the Cu_2CoSnS_4/n-Si heterojunction can be estimated. The magnitudes of V_{bi} and N for the Cu_2CoSnS_4/n-Si device are listed in Table I. Table I illustrated that the variance of built-in voltages (V_{bi}) and carrier concentration (N) with temperature for the Cu_2CoSnS_4/n-Si heterojunction. It is observable that the magnitudes of V_{bi} were reduced with raising the temperature while the magnitudes of N were increased with increasing the temperature. Actually, the interface density of charges improves by raising the temperature. It has a significant impact on the apparent built-in voltage.

Evidently, raising the interface density of charges reduces the built-in voltage. The large interface density of states likewise acts as practical tunneling centers.[21]

Table II. The heterojunction parameters evaluated from the dark *I–V* characteristics of the (Al/n-Si/Cu_2CoSnS_4/Au) heterojunction

T (K)	*n*	ϕ_b(ev)	R_S (Ω)	R_{sh} (kΩ)
308	2.68	0.785	205	52.43
323	2.47	0.812	191	43.61
343	2.31	0.843	165	35.15
353	2.19	0.875	147	31.82
373	2.06	0.893	133	28.76

Dark Current–Voltage Characterization

The dark *I–V* characteristic is very useful to determine the diode parameters like the ideality factor n, shunt resistance R_s, and the series resistance R_{sh} and barrier height ϕ_b. Figure 5 depicts the *I–V* measurements of the Al/n-Si/Cu_2CoSnS_4/Au heterojunction in the dark at various temperatures. It is observed from this curve that the *I–V* plot of the Cu_2CoSnS_4/n-Si device displays a rectification performance.

The *I–V* curve of the Al/n-Si/Cu_2CoSnS_4/Au heterojunction in the forward bias region was studied according to the thermionic emission theory by the presented relation[19,20]:

$$I = I_0\left(\exp\left(\frac{qV}{nKT}\right) - 1\right), \quad (5)$$

where n represents ideality factor, T represents the temperature in Kelvin, q represents the electronic charge, V represent applied voltage and K is the Boltzmann constant.

The reverse saturation current of the Cu_2CoSnS_4/n-Si device was estimated by the below formula[21,22]:

$$I_o = AA^*T^2 \exp\left[\frac{-q\phi_b}{KT}\right]. \quad (6)$$

Here ϕ_b represents the barrier height, A^* denotes the Richardson constant for the n-Si (which equals A^* = 122 A/cm^2 K^2)[23] and A denotes the Schottky contact area.

The magnitudes of ideality factor n, of the Al/n-Si/Cu_2CoSnS_4/Au heterojunction, was estimated from the slope of the linear plot of Fig. 5 according to the below expression[24,25]:

$$\ln(I) = \frac{qV}{nKT} + \ln(I_0). \quad (7)$$

The ideality factor values n of the Al/n-Si/Cu_2CoSnS_4/Au heterojunction are given in Table II. It is noted from Table II that the n values of the Al/n-Si/Cu_2CoSnS_4/Au heterojunction were decreased via increasing the annealed temperature. As observed the magnitudes of ideality factor n for n values of the Al/n-Si/Cu_2CoSnS_4/Au heterojunction were higher than unity. This performance occurred

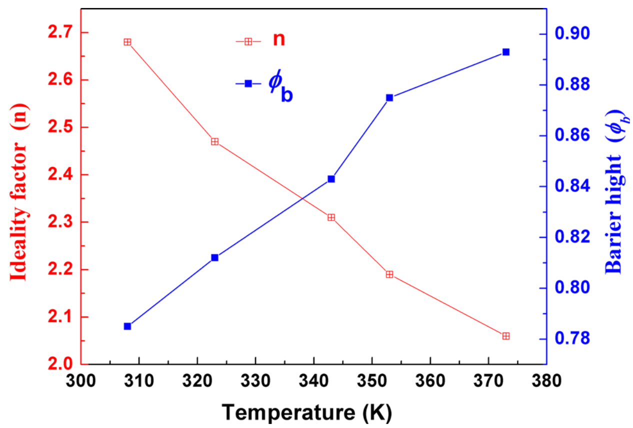

Fig. 6. Dependence of ideality factor and barrier height on temperature for the Al/n-Si/Cu_2CoSnS_4/Au heterojunction.

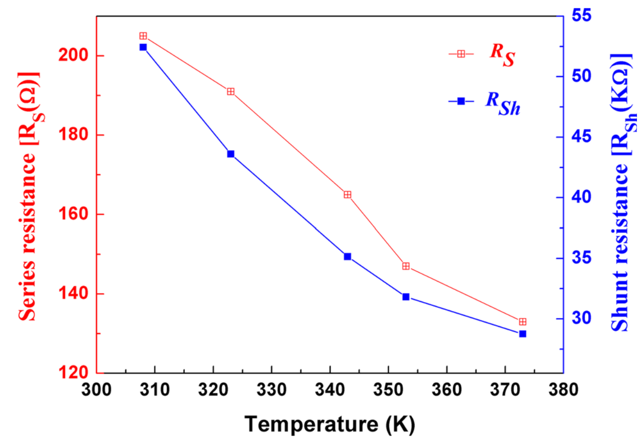

Fig. 8. Dependence of series and shunt resistances on temperature for the Al/n-Si/Cu_2CoSnS_4/Au heterojunction.

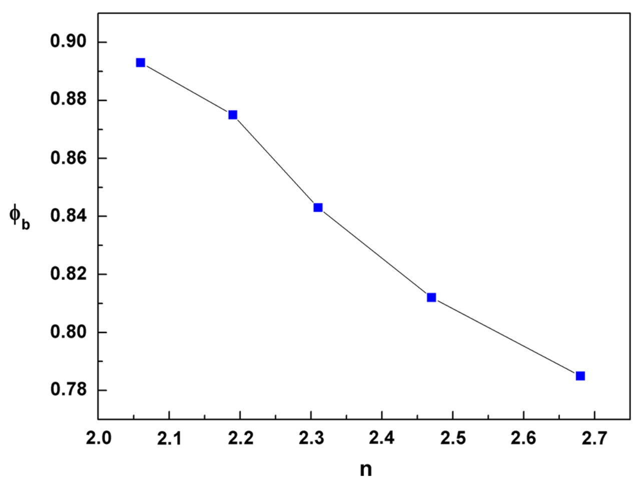

Fig. 7. Plot of the ideality factor versus barrier height for the Al/n-Si/Cu_2CoSnS_4/Au heterojunction.

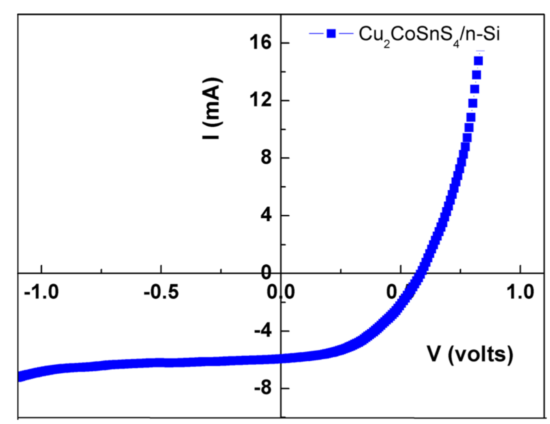

Fig. 9. The *I–V* characteristics of the Al/n-Si/Cu_2CoSnS_4/Au heterojunction under illumination.

because of increasing of the leakage current due to the recombination of the electron and holes in the depletion region.[26]

The barrier height ϕ_b at zero bias for the Al/n-Si/Cu_2CoSnS_4/Au heterojunction is given by the next relation[27,28]:

$$\phi_b = \frac{K_B T}{q} \ln\left(\frac{AA^* T^2}{I_0}\right). \tag{8}$$

The magnitudes of barrier height ϕ_b of the Al/n-Si/Cu_2CoSnS_4/Au heterojunction are listed in Table II.

Figure 6 presents the temperature effect on the ϕ_b and n of the Al/n-Si/Cu_2CoSnS_4/Au heterojunction. By raising the annealing temperature on the Al/n-Si/Cu_2CoSnS_4/Au heterojunction, the ϕ_b values were increased while the n values were decreased. This performance is in agreement with various articles like Farag[29] and agree with Uluşan.[30]

The relation between the ideality factor n and the barrier height ϕ_b for the Al/n-Si/Cu_2CoSnS_4/Au heterojunction is presented in Fig. 7. It is observed from this plot that the magnitudes of the ideality factor n increase as the barrier height ϕ_b decreases.

The series resistance R_S of the Al/n-Si/Cu_2CoSnS_4/Au heterojunction was estimated via the slope of the linear plot of the forward *I–V* plot according to the following relation[31]:

$$R_S = \frac{\Delta V_{\text{Forward Bias}}}{\Delta I_{\text{Forward Bias}}}. \tag{9}$$

While the magnitude of shunt resistance R_{Sh} for the Al/n-Si/Cu_2CoSnS_4/Au heterojunction was evaluated via the slope of the linear plot of the reverse *I–V* plot according to the following expression[30]:

$$R_{Sh} = \frac{\Delta V_{\text{Reverse Bias}}}{\Delta I_{\text{Reverse Bias}}}. \tag{10}$$

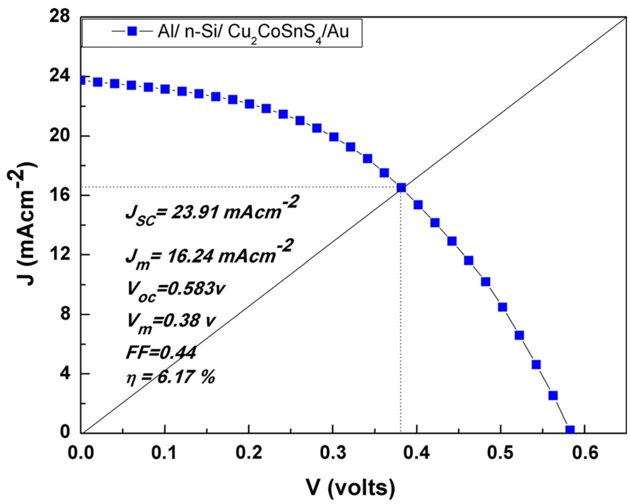

Fig. 10. The J–V characteristics for the Al/n-Si/Cu_2CoSnS_4/Au heterojunction under illumination of 100 mW cm^{-2}.

Figure 8 displays the temperature effect on the magnitudes of the shunt resistance R_{Sh} and the series resistance R_S for the Al/n-Si/Cu_2CoSnS_4/Au heterojunction. There is an enhancement in the conductivity of the fabricated device resulting from the decreasing of R_S and R_{Sh} with increasing the temperature.[32] The magnitudes of R_S and R_{Sh} are given in Table II.

Photovoltaic Analysis of the Al/n-Si/Cu_2CoSnS_4/Au

The photovoltaic analysis of the Al/n-Si/Cu_2CoSnS_4/Au heterojunction has been investigated via determining the I–V characteristics below the illumination conditions. The illuminated I–V curve of the Al/n-Si/Cu_2CoSnS_4/Au heterojunction is presented in Fig. 9. As observed the current values of the Al/n-Si/Cu_2CoSnS_4/Au heterojunction under illumination conditions was higher than the current values in the dark. This performance is owing to the production of electron–hole pairs.[33–35]

Figure 10 depicts the J–V curve of the Al/n-Si/Cu_2CoSnS_4/Au heterojunction. Moreover, the photovoltaic constants of the prepared heterojunction as J_{SC}= 23.91 mA cm^{-2}, J_m = 16.24 mA cm^{-2}, V_{OC}= 0.583 V, V_m = 0.38 V and the efficiency were estimated via this plot.

The magnitudes of the device efficiency (η) and fill factor of the Al/n-Si/Cu_2CoSnS_4/Au heterojunction have been evaluated according to the below relations[36,37]:

$$\eta = \frac{P_{max}}{P_{in}} = \frac{FF \times V_{OC} \times J_{SC}}{P_{in}} \times 100\%, \qquad (11)$$

$$FF = \frac{V_m \times J_m}{V_{oc} \times J_{sc}}, \qquad (12)$$

where P_{in} denotes the input energy from the sun, P_{max} denotes the output energy from the device, FF is the fill factor, J_{sc} is the short-circuit current density and V_{oc} represents the open-circuit voltage. The magnitudes of the FF and the η of the Al/n-Si/Cu_2CoSnS_4/Au heterojunction were 0.44% and 6.17% respectively.

CONCLUSION

In the present study, Cu_2CoSnS_4 thin film was sprayed on the n-Si via spray pyrolysis technique. The formation of the Cu_2CoSnS_4 film was confirmed by XRD and FE-SEM. The Cu_2CoSnS_4 thin films are polycrystalline. The EDX pattern displays that the Cu_2CoSnS_4 thin film is near stoichiometric in composition. The Capacitance- Voltage study of the Cu_2CoSnS_4/n-Si heterojunction displays that the junction nature is an abrupt junction. The diode parameters of the Cu_2CoSnS_4/n-Si heterojunction were determined by investigating temperature dependences of the I–V characteristics. By increasing the temperature, the magnitudes of the barrier height ϕ_b of the Cu_2CoSnS_4/n-Si heterojunction increases while the magnitudes of the ideality factor n, shunt resistance R_{Sh} and series resistance R_S were decreased. The photovoltaic constants of the Cu_2CoSnS_4/n-Si heterojunction were evaluated for display efficiency of 6.17%.

REFERENCES

1. S. Siebentritt and S. Schorr, *J. Prog. Photovolt.* 20, 512 (2012). https://doi.org/10.1002/pip.2156.
2. M. Nakashima, T. Yamaguchi, S. Yukawa, J. Sasano, and M. Izaki, *J. Thin Solid Films* 621, 47 (2017). https://doi.org/10.1016/j.tsf.2016.11.035.
3. A. Walsh, S. Chen, S.-H. Wei, and X.-G. Gong, *Adv. Eng. Mater.* 2, 400 (2012). https://doi.org/10.1002/aenm.201100630.
4. S.S. Fouad, I.M. El Radaf, P. Sharma, and M.S. El-Bana, *J. Alloys Compd.* 757, 124 (2018). https://doi.org/10.1016/j.jallcom.2018.05.033.
5. A. Ennaoui, M. Lux-Steiner, A. Weber, D. Abou-Ras, I. Kötschau, H.-W. Schock, R. Schurr, A. Hölzing, S. Jost, and R. Hock, *J. Thin Solid Films* 517, 2511 (2009). https://doi.org/10.1016/j.tsf.2008.11.061.
6. T.K. Todorov, J. Tang, S. Bag, O. Gunawan, T. Gokmen, Y. Zhu, and D.B. Mitzi, *Adv. Eng. Mater.* 3, 34 (2013). https://doi.org/10.1002/aenm.201200348.
7. Y. Cui, R. Deng, G. Wang, and D. Pan, *J. Mater. Chem.* 22, 23136 (2012). https://doi.org/10.1039/C2JM33574C.
8. P.S. Maldar, A.A. Mane, S.S. Nikam, S.D. Giri, A. Sarkar, and A.V. Moholkar, *J. Mater. Sci. Mater. Electron.* 28, 18891 (2017). https://doi.org/10.1007/s10854-017-7842-1.
9. C. An, K. Tang, G. Shen, C. Wang, L. Huang, and Y. Qian, *Mater. Res. Bull.* 38, 823 (2003). https://doi.org/10.1016/S0025-5408(03)00046-1.
10. J.Y. Chane-Ching, A. Gillorin, O. Zaberca, A. Balocchi, and X. Marie, *Chem. Commun.* 47, 5229 (2011). https://doi.org/10.1039/C1CC10749F.
11. B. Murali, M. Madhuri, and S.B. Krupanidhi, *Cryst. Growth* 14, 3685 (2014). https://doi.org/10.1021/cg500622f.
12. A. Gupta, K. Mokurala, A. Kamble, S. Shankar, S. Mallick, and P. Bhargava, *AIP Conf. Proc.* 1665, 140022 (2015).
13. A.M. Mansour, I.S. Yahia, and I.M. El Radaf, *Mater. Res. Express* 5, 076406 (2018). https://doi.org/10.1088/2053-1591/aad15b.

14. P.S. Maldara, M.A. Gaikwada, A.A. Manea, S.S. Nikama, S.P. Desaia, S.D. Girib, A. Sarkarb, and A.V. Moholkara, *J. Solar Energy* 158, 89 (2017). https://doi.org/10.1016/j.solener.2017.09.036.
15. M. Krishnaiah, R.K. Mishra, S.G. Seo, S.H. Jin, and J.T. Park, *J. Alloys Compd.* 781, 1091 (2019). https://doi.org/10.1016/j.jallcom.2018.12.036.
16. M.S. El-Bana, I.M. El Radaf, S.S. Fouad, and G.B. Sakr, *J. Alloys Compd.* 705, 333 (2017). https://doi.org/10.1016/j.jallcom.2017.02.106.
17. I.M. El Radaf and R.M. Abdelhameed, *J. Alloys Compd.* 765, 1174 (2018). https://doi.org/10.1016/j.jallcom.2018.06.277.
18. I.M. El Radaf, S.S. Fouad, A.M. Ismail, and G.B. Sakr, *Mater. Res. Express* 5, 046406 (2018). https://doi.org/10.1088/2053-1591/aaba0a.
19. A. Ashery, A.A.M. Farag, and M. Zeama, *Superlattices Microstruct.* 66, 136 (2014). https://doi.org/10.1016/j.spmi.2013.12.002.
20. T.A. Hameed, I.M. El Radaf, and H.E. Elsayed-Ali, *J. Mater. Sci. Mater. Electron.* 29, 12584 (2018). https://doi.org/10.1007/s10854-018-9375-7.
21. M. Nasr, A.M. Mansour, and I.M. El Radaf, *Mater. Res. Express* 6, 036405 (2019). https://doi.org/10.1088/2053-1591/aaf3f3.
22. I.S. Yahia, A.A.M. Farag, F. Yakuphanoglu, and W.A. Farooq, *Synth. Met.* 161, 881 (2011). https://doi.org/10.1016/j.synthmet.2011.02.016.
23. R.K. Gupta, M.E. Aydın, and F. Yakuphanoglu, *Synth. Met.* 161, 2355 (2001). https://doi.org/10.1016/j.synthmet.2011.09.002.
24. A. Ashery, I.M. El-Radaf, and M.M.M. Elnasharty, *J. Silicon* 1876, 9918 (2018). https://doi.org/10.1007/s12633-018-0047-2.
25. I.M. El Radaf, M.S. Al-Kotb, M. Nasr, and I.S. Yahia, *J. Alloys Compd.* 788, 206 (2019). https://doi.org/10.1016/j.jallcom.2019.02.189.
26. A.A.M. Farag and I.S. Yahia, *Synth. Met.* 161, 32 (2011). https://doi.org/10.1016/j.synthmet.2010.10.030.
27. I.M. El Radaf, A.M. Mansour, and G.B. Sakr, *J. Semicond.* 39, 124010 (2018). https://doi.org/10.1088/1674-4926/39/12/124010.
28. İ. Taşçıoğlu, S.O. Tan, F. Yakuphanoğlu, and Ş. Altındal, *J. Electron. Mater.* 47, 6059 (2018). https://doi.org/10.1007/s11664-018-6495-z.
29. V. Ganesh, M.A. Manthrammel, M. Shkir, I.S. Yahia, H.Y. Zahran, F. Yakuphanoglu, and S. AlFaify, *Appl. Phys.* 124, 424 (2018). https://doi.org/10.1007/s00339-018-1832-x.
30. B. Saha, K. Sarkar, A. Bera, K. Deb, and R. Thapa, *Appl. Surf. Sci.* 418, 328 (2017). https://doi.org/10.1016/j.apsusc.2017.01.142.
31. G.K. Rao, *Appl. Phys. A* 224, 1 (2017). https://doi.org/10.1007/s00339-017-0850-4.
32. A.A.M. Farag, I.S. Yahia, and M. Fadel, *Int. J. Hydrog. Eng.* 34, 4906 (2009). https://doi.org/10.1016/j.ijhydene.2009.03.034.
33. A.B. Uluşan, A. Tataroglu, Y. Azizian-Kalandaragh, and S. Altınd, *Mater. Sci. Mater. Electron.* 29, 159 (2018). https://doi.org/10.1007/s10854-017-7900-8.
34. I.M. El Radaf, M. Nasr, and A.M. Mansour, *Mater. Res. Express* 5, 015904 (2018). https://doi.org/10.1088/2053-1591/aaa25e.
35. A.A.M. Farag, F.S. Terra, A. Ashery, and A.M. Mansour, *J. Alloys Compd.* 615, 604 (2014). https://doi.org/10.1016/j.jallcom.2014.06.058.
36. I.M. El Radaf, T.A. Hamid, and I.S. Yahia, *J. Mater. Res. Express* 5, 066416 (2018). https://doi.org/10.1088/2053-1591/aaca7b.
37. M. Nasr, I.M. El Radaf, and A.M. Mansour, *J. Phys. Chem. Solids* 115, 283 (2018). https://doi.org/10.1016/j.jpcs.2017.12.029.

Publisher's Note Springer Nature remains neutral with regard to jurisdictional claims in published maps and institutional affiliations.